scientific reports

Check for updates

OPEN

Development of a novel multi-epitope subunit mRNA vaccine candidate to combat *Acinetobacter baumannii*

Shiyang Ma[1,2,3,4,5], Fei Zhu[1,2,3,4,5], Peipei Zhang[1,2,3,4,5], Yizhong Xu[1,2,3,4,5], Ziyou Zhou[1,2,3,4,5], Hang Yang[1,2,3,4,5], Caixia Tan[6], Jie Chen[1,2,3,4,5]✉ & Pinhua Pan[1,2,3,4,5]✉

***Acinetobacter baumannii*, an opportunistic bacterium prevalent in various environment, is a significant cause of nosocomial infections in ICUs. As the causative agent of pneumonia, septicemia, and meningitis, *A. baumannii* typically exhibits multidrug resistance and is associated with poor prognosis, thus led to a challenge for researchers in developing new treatment and prevention methods. This study involved the development of a novel multi-epitope mRNA vaccine for *A. baumannii* and validation of in silico approaches was conducted. We screened 11 immunodominant epitopes for cytotoxic T cells, 5 for helper T cells, and 10 for Linear B-cell based on promising candidate proteins omp33-36, ompA and ompW, the selection of these three proteins is based on reverse vaccinology screening and previous work by other researchers. All predicted epitopes demonstrated strong antigenicity, immunogenicity without posing any potential harm to humans. Additionally, high conservancy is required to cover different strains. All epitopes, as well as adjuvants, were constructed into a final vaccine, which was further assessed by calculating its physicochemical properties. Next, we docked the vaccine protein with immune receptors and analyzed the complexes with dynamic simulations to evaluate its affinity to receptors. At last, the constructed sequence is translated to an mRNA sequence. The results indicated the constructed vaccine is capability of eliciting robust humoral and cellular immune responses, making it a promising candidate for protection against the targeted pathogen.**

Keywords *Acinetobacter baumannii*, Multiepitope vaccine, Molecular docking, Molecular dynamics, mRNA vaccine

Acinetobacter baumannii is one of the six ESKAPE pathogens, these bacteria have developed resistance to commonly used antibiotics, posing an increasing threaten to public health[1]. Described as a successful pathogen, *A. baum*annii is widely prevalent in the environment, spanning from soil to water[2], with the ability to colonize skin, respiratory tracts, or wounds[3]. It typically incites infections in debilitated patients, resulting in various clinical presentations including ventilator-associated pneumonia (VAP), bloodstream infections, respiratory ailments, urinary tract infections, gastrointestinal infections, and sepsis tied to prolonged medical device utilization[4]. The emergence of *Acinetobacter baumannii* as a pressing threat stem from its resistance to various antibiotics, particularly carbapenems[5]. This resistance is underpinned by a repertoire of mechanisms encompassing β-lactamases, aminoglycoside-modifying enzymes, permeability deficiencies, efflux pumps, and alterations in target sites[6,7]. Out of the 1,011 strains gathered from 48 countries, it is evident that over half of them exhibit multidrug-resistant (MDR) properties[8]. *Acinetobacter baumannii* infections have inflicted significant harm on global public health, with infection rates ranging from 2 to 4% of all medical-related infections and

[1]Department of Respiratory Medicine, National Key Clinical Specialty, Branch of National Clinical Research Center for Respiratory Disease, Xiangya Hospital, Central South University, Changsha 410008, Hunan, China. [2]Center of Respiratory Medicine, Xiangya Hospital, Central South University, Changsha 410008, Hunan, China. [3]Clinical Research Center for Respiratory Diseases in Hunan Province, Changsha 410008, Hunan, China. [4]Hunan Engineering Research Center for Intelligent Diagnosis and Treatment of Respiratory Disease, Changsha 410008, Hunan, China. [5]National Clinical Research Center for Geriatric Disorders, Xiangya Hospital, Changsha 410008, Hunan, P.R. China. [6]Department of Infection Control Center of Xiangya Hospital, Central South University, Changsha 410008, Hunan, China. ✉email: chenjie869@csu.edu.cn; pinhuapan668@csu.edu.cn

exceeding 10% in intensive care units (ICUs), moreover, the mortality rate due to MDR cases exceeds 50%[9–11]. Given the lack of substantial therapeutic agents, non-antibiotic strategies, such as vaccines, are essential for subsequent prevention.

Over the past decade, various strategies have been explored to develop an effective vaccine against A.baumannii, such as whole-cell vaccines, subunit vaccines, multicomponent vaccines, and nucleic acid vaccines. Despite the research conducted, none of these methods progressed to clinical trials[10,12]. Traditional vaccine development relies heavily on empirical knowledge and requires significant time and labor investment. However, with the rise of immunoinformatics methods, in silico vaccine design is emerging as a promising new approach[13]. To date, efforts have been made to develop vaccines for various pathogens such as bacteria, viruses, parasites, and tumors[14], among which most are about COVID-19. Otherwise, multiepitope vaccines created using in silico methods have elicited robust immune responses against Group B Streptococcus[15] and *EBV* infections[16], showcasing the efficacy of epitope vaccines designed in silico.

In this study, we have selected core proteins of *Acinetobacter baumannii* through reverse vaccinology analysis and chosen three target proteins based on some existing studies. Outer membrane protein A (OmpA), Outer membrane W (OmpW), and Outer membrane protein33-36 (Omp33-36) were selected for additional prediction of immunodominant epitopes. Outer membrane proteins (OMPs) are a series of β-barrel structured proteins anchored in the outer membrane of *A. baumannii*. Several OMPs' are introduced as appropriate vaccine candidates, vaccination with outer membrane vesicles has the ability to protect disseminated sepsis[17]. Outer membrane protein A (OmpA) is among the most plentiful outer membrane proteins (OMPs) and exhibits remarkable potential as a therapeutic target[18]. Recombinant OmpA (rOmpA) with aluminum hydroxide adjuvant can enhance survival rates of infected mice[19], and mucosal immunization with rOmpA can decrease mortality caused by *A. baumannii*[20]. Further, in a pneumonia mouse model, a DNA vaccine encoding OmpA demonstrated significant defensive efficacy[21]. Meanwhile, OmpW and Omp33-36 are highly associated with adherence and invasion, and are considered as important virulence factor of *A. baumannii*. Meanwhile, OmpW and Omp33-36 are highly conversed among *A. baumannii* strains, OmpW is conserved in 804 strains with over 91% identity. While the conservation rate for Omp33-36 exceeds 98% across more than 1600 strains of *Acinetobacter baumannii*[22]. OmpW is another potential target for inducing protective immune response against *A. baumannii* infection, which can elicit strong specific antibodies and rescue mice from deadly sepsis[23]. While Omp33-36 is highly associated with adherence and invasion, and is considered an important virulence factor of *A. baumannii*, which make Omp33-36 another promising target for vaccine development[24].

Since little progress have been made for developing *A. baumannii* vaccine, in this study, we developed a multi-epitope vaccine (MEV) and designed its form into epitope-based mRNA vaccine. mRNA serves as an optimal vaccine platform due to its distinct advantages in enhancing efficacy, shortening development time, ensuring safety, and minimizing manufacturing costs[25]. Further, the efficacy of the vaccine has been verified through in silico methods including molecular docking and molecular dynamics simulations. Results indicated this MEV to be a promising candidate in combating *A. baumannii* infection.

Results

Identification of target proteins

Firstly, we collected 95 fully sequenced genomes of *Acinetobacter baumannii* from the NCBI database and analyzed for core genes with USEARCH clustering algorithm of BPGA. A total of 8701 genes were identified, out of which 1965 were classified as core proteins (Fig. 1A). The distribution analysis based on clusters of orthologous groups (COG) revealed that the majority of core genes are involved in metabolism and information storage and processing (Fig. 1B). Subsequently, the core proteome was subjected to a homology filter, which led to the identification of 694 proteins as non-homologous to humans. This filtering process aims to prevent cross-reactivity of vaccine candidates with the human host, thereby reducing the risk of autoimmunity. To identify potential target proteins for vaccine development, we evaluated the antigenicity and toxicity of the 694 proteins. Proteins with more than 230 amino acids and less than 2 transmembrane helices were deemed more suitable for serving as target proteins in vaccine design. Ultimately, three outer membrane proteins, namely OmpW, OmpA, and Omp33-36, were selected for further epitope prediction.

To further confirm that the vaccines designed against these three target proteins can cover a wider range of strains, we collected all the reference sequences of OmpA(507 sequences), OmpW(379 sequences) and Omp33-36(47 sequences) from different strains in the NCBI database and drew phylogenetic trees. The results showed that the phylogenetic trees of the three proteins were assembled together to form a single branch and were closely related to each other (Fig. 1 C, D, E). Therefore, the *Acinetobacter baumannii* vaccines designed against OmpA, OmpW and Omp33-36, may be effective against all strains.

Mapping of epitopes

Sequences for epitope prediction were retrieved from the NCBI database using various selection tools. A total of 11 cytotoxic T lymphocyte (CTL) epitopes (Table 1), 5 helper T lymphocyte (HTL) epitopes (Table 2), and 10 linear B cell epitopes (Table 3) were identified as potential candidates for further vaccine design. All the predicted epitopes exhibited high antigenicity, conservation, and were non-toxic. Additionally, the helper T lymphocyte epitopes were expected to induce the production of interleukin-2 (IL-2), interferon-gamma (IFN-g), and interleukin-4 (IL-4).

Construction of the MEV and physicochemical properties prediction

The MEV sequence comprises 11 CTL epitopes, 5 HTL epitopes and a PADRE sequence, and 10 linear B cell epitopes. A β-defensin is attached to the N-terminus, and a P30 peptide is attached to the C-terminus as adjuvants (Fig. 2A). The total sequence consists of 516 amino acids (AAs), and has a molecular weight of 55.1 kDa,

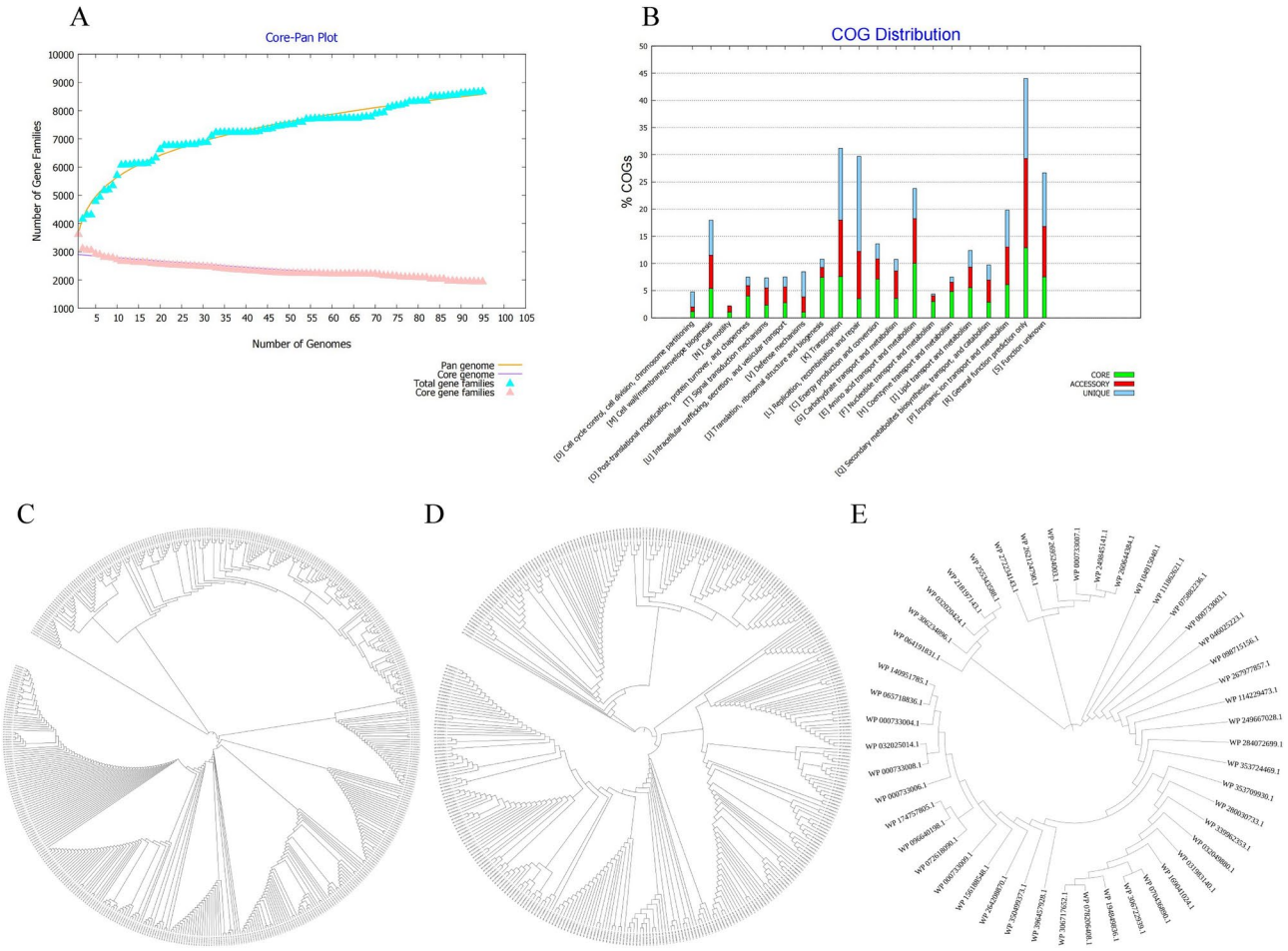

Fig. 1. Analyze of core proteins of *A. baumannii* genome. (**A**) Core-Pan Plot of *A. baumannii* (**B**) COG distribution plot of *A. baumannii*. (**C**) Phylogenetic tree of OmpA (**D**) Phylogenetic tree of OmpW (**E**) Phylogenetic tree of Omp33-36.

with a theoretical isoelectric point (pI) of 9.45, falling within an appropriate range for vaccine development. The predicted overall protective antigenicity of the protein is 0.7814 (>0.4), indicating robust antigenicity. Additionally, it is forecasted to be soluble with a 0.7015 probability upon overexpression. Notably, the vaccine exhibits no allergenicity based on testing with the AllerTOP 2.0 and AllerFP servers, and no toxicity according to the ToxinPred 2.0 analysis. The protein has a half-life of approximately 30 h in mammalian reticulocytes and over 10 h in Escherichia coli. Additionally, the instability index (II) for the protein is computed at 32.9, indicating its classification as stable, and the protein's grand average of hydropathicity (GRAVY) is calculated as -0.085, this proves that the protein has hydrophilicity.

Secondary and tertiary structure prediction and validation

The GOR4 server predicted the MEV's secondary structure, showing that the sequence comprises 28.29% alpha helix, 19.57% extended strand, and 52.13% random coil (Fig. 2B). Subsequently, the Robetta software was used to predict and generate the MEV's tertiary structure, and GalaxyRefine refined the structure by optimizing the structure's side chains (Fig. 2C). The Prosa analysis yielded a Z-score of -6.32, indicating the model has a high stereochemical quality (Fig. 2F). Evaluation by the Procheck server indicated that the protein structure had an overall high quality, with Ramachandra plots revealing that 84.7% of residues were in the most favored regions, 11.8% in additional regions, 2.9% in generously allowed regions, and only 0.7% in disallowed regions (Fig. 2E). Additionally, ERRAT predicted a favorable score of 92.899 for the vaccine's tertiary structure (Fig. 2D).

Conformational B cell epitopes prediction

After analyzing the MEV's third structure, ElliPro identified 8 conformational B cell epitopes, their locations on the structure are depicted in Figure S1. The overall scores of conformational epitopes are ranging from 0.862 to 0.685(Table S1).

Protein	Supertype	Comb Score	Epitope Sequence	Start Position	Antigenicity	Immunogenicity	Allergic	Toxicity	MHC alle	Score	RANK	Conservatism
omp33-36	A2	1.2892	AMLLPNFLV	140	1.652	0.06067	-	-	HLA-A*02:01	0.487874	0.27	73.50%
									HLA-A*02:06	0.325128	0.52	
	A2	1.0778	MLLPNFLVA	141	1.8157	0.1039	-	-	HLA-A*02:01	0.43892	0.32	74%
									HLA-A*02:06	0.431263	0.34	
									HLA-A*02:03	0.303221	0.49	
	A3	0.7553	TAQGTYYFK	43	0.6349	0.0961	-	-	HLA-A*68:01	0.737512	0.27	76.60%
									HLA-A*11:01	0.683033	0.15	
									HLA-A*30:01	0.280933	0.47	
	A2	1.3642	YLPTPYLPV	101	1.5300	0.00534	-	-	HLA-A*02:01	0.612748	0.19	77.30%
									HLA-A*02:03	0.609665	0.15	
									HLA-A*02:06	0.518073	0.23	
ompA	B7	1.2584	APVEPTPVA	208	0.8366	0.15465	-	-	HLA-B*07:02	0.706448	0.12	86.60%
									HLA-B*35:01	0.425488	0.3	
									HLA-B*51:01	0.227872	0.62	
	B7	1.4646	APVVEVAPV	202	0.7076	0.21784	-	-	HLA-B*07:02	0.706448	0.12	86.20%
									HLA-B*35:01	0.425488	0.3	
									HLA-B*51:01	0.227872	0.62	
	A24	0.8155	TPLLLGYTF	27	0.7926	0.0259	-	-	HLA-B*35:01	0.931458	0.03	85.10%
	B7	1.0154							HLA-B*53:01	0.858236	0.03	
	B8	0.8272							HLA-B*07:02	0.464045	0.28	
									HLA-B*51:01	0.395896	0.31	
									HLA-B*08:01	0.199931	0.59	
ompW	A1	1.5173	FTAGFTYDF	308	1.267	0.20718	-	-	HLA-B*35:01	0.931458	0.03	79%
	A26	0.9392							HLA-B*53:01	0.858236	0.03	
	B39	0.8421							HLA-B*07:02	0.464045	0.28	
	B58	1.3734							HLA-B*51:01	0.395896	0.31	
	B62	1.1451							HLA-B*08:01	0.199931	0.59	
	A1	0.7653	PIFTAGFTY	306	0.9135	0.26854	-	-	HLA-A*30:02	0.283861	0.5	77.30%
	B62	0.8634							HLA-B*15:01	0.20238	0.94	
	B7	1.3126	SVRAWTPAI	218	0.879	0.32191	-	-	HLA-A*30:01	0.463672	0.16	79%
	B62	1.042							HLA-B*07:02	0.26475	0.53	
									HLA-A*32:01	0.205096	0.37	
	B39	0.9493	VSAGWLHVM	31	0.4859	0.30348	-	-	HLA-B*57:01	0.52163	0.51	88.30%
	B58	1.2095							HLA-B*58:01	0.442387	0.38	
	B62	0.9596							HLA-A*32:01	0.151002	0.5	
									HLA-B*35:01	0.107783	0.98	

Table 1. Screening of CTL epitopes.

Disulfide engineering of the vaccine construct

Through the prediction by the Disulfide by Design 2.13 tool, we found that there are three existing pairs of disulfide bonds in the vaccine sequence, namely CYS8—CYS37, CYS15—CYS30, and CYS20—CYS38(Figure S2). These three pairs of residues can form natural disulfide bonds and meet the conditions that the χ3 angle is within the range of -87° or + 97° ± 10°, the Cα—Cβ—Sγ angle is within the range of 114.6° ± 10°, and the energy value is lower than 2.2 kcal/mol(Table S2).

Molecular docking

The refined vaccine structure was further examined for its affinity with immune receptors TLR2 (Fig. 3) and TLR4 (Fig. 4). Molecular docking was conducted with Cluspro tool, and the docking results were refined using the HADDOCK 2.4 server. Table S3 presents the detailed docking parameters, and the results with low HADDOCK scores indicate a successful interaction between the vaccine and the receptors. The docking results were visualized in Figs. 4 and 5 using PyMOL software and further analyzed for interactions between the receptor and ligand using PDBsum. The analyze uncovered the existence of numerous H-bonds and salt bridges.

Molecular dynamic simulation

We conducted a 100 ns molecular dynamic simulation with Gromacs v2022.1 to investigate the stability of MEV-receptor complexes in the human body. Root Mean Square Deviation (RMSD) assesses the variance between the simulated and experimental molecular structures. A lower RMSD value indicates a closer match between the simulation and experimental results. The RMSD plot serves as a tool to monitor the structural fluctuations of the MEV-TLR complexes. Figure 5A illustrates that the RMSD of the MEV-TLR2 complex increased rapidly within the time range of 0—5 ns, fluctuated before 40 ns, and then tended to stabilize, while the complex of MEV-TLR4 while the RMSD of the MEV-TLR4 complex increased gently before 50 ns and then remained stable as well. The average RMSD of MEV-TLR2 is 0.86, and the average RMSD of MEV-TLR4 is 0.85, indicating that both complexes maintained a stable binding. The Radius of Gyration (Rg) is a crucial parameter that defines the molecular's size and shape. Smaller Rg correspond to more compact structure, whereas larger Rg indicates more extended structure. Therefore, the compactness of protein structures can be evaluated by analyzing Rg plots. According to Fig. 5B, the Rg of MEV-TLR4 in the system reaches equilibrium at 10 ns, initiating a steady descent. Meanwhile, the Rg of MEV-TLR2 fluctuates and reduces by 4.0 nm, stabilizing after 50 ns. These observations suggest that both complexes became more compact throughout the 100 ns simulation. The average Rg is 4.00 for MEV-TLR2 and 3.37 for MEV-TLR4 complex. Root Mean Square Fluctuation (RMSF) assesses the level of fluctuation in atom positions within a molecule, with lower RMSF indicating increased stability in movements throughout the simulation process. RMSF values of receptors and ligands were illustrated in Fig. 5C and Fig. 5D separately. All residues in complex of vaccine-TLR2 exhibit lower flexibility while in the vaccine-TLR4 complex, residue 420–480 exhibit relatively higher flexibility. Overall, the vaccine proteins and TLR molecules consistently maintained stable states, suggesting high binding affinities between the ligand and receptor molecules. Moreover, the number of hydrogen bonds serves as a measure of the interaction strength between the receptor and ligand proteins; a higher number of hydrogen bonds indicates a stronger interaction (Fig. 5E). Throughout the 100 ns simulation, the hydrogen bonds in both complexes tended to increase, further confirming the strengthening of interactions.

Furthermore, GMX_MMPBSA evaluated the binding energies from the final 20 ns of molecular dynamics simulation trajectories. The resulting binding energies for the vaccine interactions with TLR2(-196.44 kJ/mol) and TLR4(-239.26 kJ/mol). These findings further illustrate that the MEV effectively engages with immune receptors, leading to the stimulation of host immune responses (Table S4).

Population coverage and immunization simulation

The MEV's population coverage is determined by evaluating epitopes and their respective MHC alleles, as distinct ethnics exhibit varying frequencies in MHC distribution. The IEDB server calculation demonstrated that multi-epitope vaccines offered coverage to 99.67% of the worldwide population (Figure S3).

The C-IMMSIM simulates the host's immune response to vaccine antigens. In a 35 days short simulation of the human immune response, antibody levels progressively increase after three vaccine injections, peaking at nearly 600,000. After 25 days, the antibodies began to decrease, we anticipate that over a longer period of time, the levels of antibodies will reach a stable state and remain elevated in the long term (Fig. 6A). Furthermore, three vaccine injections can elevate the levels of IL2 and IFN-γ in the host (Fig. 6B). Figures depict that B cells, plasma cells, and helper T cells populations sequentially increase during the three vaccine injections (Fig. 6C, 6D, 6E). Meanwhile, Resting TC cells are continuously activated by the stimulation of the vaccine (Fig. 6F), while the population of DC cells and NK cells show an initial increase post-vaccination, followed by a subsequent decline (Fig. 6G, 6H, 6I). The simulation results suggest that the MEV can induce a strong production of antibodies in the host, potentially leading to long-lasting immunity. However, further experimental validation is necessary to confirm its protective efficacy.

Construction of mRNA vaccine and vaccine vector

Through the improvement process of Jcat server, a 2394 bp cDNA sequence was obtained after reverse translation and optimization, containing the MEV sequence, Kozak, MITD along with tPA sequences. This cDNA fragment has a codon adaptation index (CAI) value of 0.99 while its GC content is 51.75%, both falling within the optimal range, indicating favorable density and thermostability. Upon merging with the UTR sequence, the MEV DNA spans 2642 bps. Subsequently, RNAfold analysis revealed a free energy of the thermodynamic ensemble of -884.82 kcal/mol (Figure S4). The predicted results suggest the mRNA vaccine to be stable. Eventually, the DNA

Protein	Start position	Epitope Sequence	MHC alle	score	Rank	Antigenicity	Immunology	Allergic	Toxicity	INF-γ	IL-4	conservatism
omp33-36	9	AVLLAMTGAHAYQFE	HLA-DRB1*12:01	0.5635	1.3	0.6316	95.25	-	-	+	+	93.50%
ompA	154	GVGAFWRLNDALSLR	HLA-DRB3*02:02	0.7928	0.21	0.9416	96.3186	-	-	+	+	79.90%
			HLA-DRB1*04:01	0.6731	1.6							
	119	IKPYVLLGAGHYKYD	HLA-DRB5*01:01	0.6161	0.56	0.5389	85.2259	-	-	+	+	83.10%
			HLA-DRB1*12:01	0.5912	1.1							
			HLA-DRB1*01:01	0.7062	1.6							
ompW	42	GKANPFNINTSVKNG	HLA-DRB3*02:02	0.9806	0.01	1.0637	69.646	-	-	+	+	85%
	245	GVGLMYAHFNDIKLN	HLA-DPA1*02:01/DPB1*01:01	0.4395	0.04	0.979	82.6942	-	-	+	+	78%
			HLA-DPA1*01:03/DPB1*04:01	0.7634	0.09							
			HLA-DPA1*03:01/DPB1*04:02	0.5187	0.13							
			HLA-DPA1*01:03/DPB1*02:01	0.7862	0.26							
			HLA-DPA1*02:01/DPB1*05:01	0.1653	0.43							
			HLA-DQA1*01:01/DQB1*05:01	0.0245	1.8							

Table 2. Screening of HTL epitopes.

Protein	Start position	Epitope	Score	Antigenicity	Allergenicity	Toxicity	Conservative
omp33-36	41	TGTAQGTYYFKNVDAS	0.95	0.9292	-	-	83.60%
	178	SVAIDEKQDAVTARTK	0.9	0.962	-	-	77.70%
ompA	197	HLKPAAPVVEVAPVEP	0.9	0.6759	-	-	85.90%
	203	PVVEVAPVEPTPVAPQ	0.89	0.7395	-	-	85.90%
	323	EGRAMNRRVFATITGS	0.84	0.7388	-	-	84.90%
	66	GIELTPWLGFEAEYNQ	0.83	0.8516	-	-	86.40%
ompW	31	VSAGWLHVMPQGKANP	0.85	0.4358	-	-	85.50%
	223	TPAIEAQYQFGKSGVN	0.85	0.7566	-	-	83%
	37	HVMPQGKANPFNINTS	0.81	0.5481	-	-	82%
	305	APIFTAGFTYDFNDSW	0.8	0.633	-	-	785

Table 3. Screening of linear B cell epitopes.

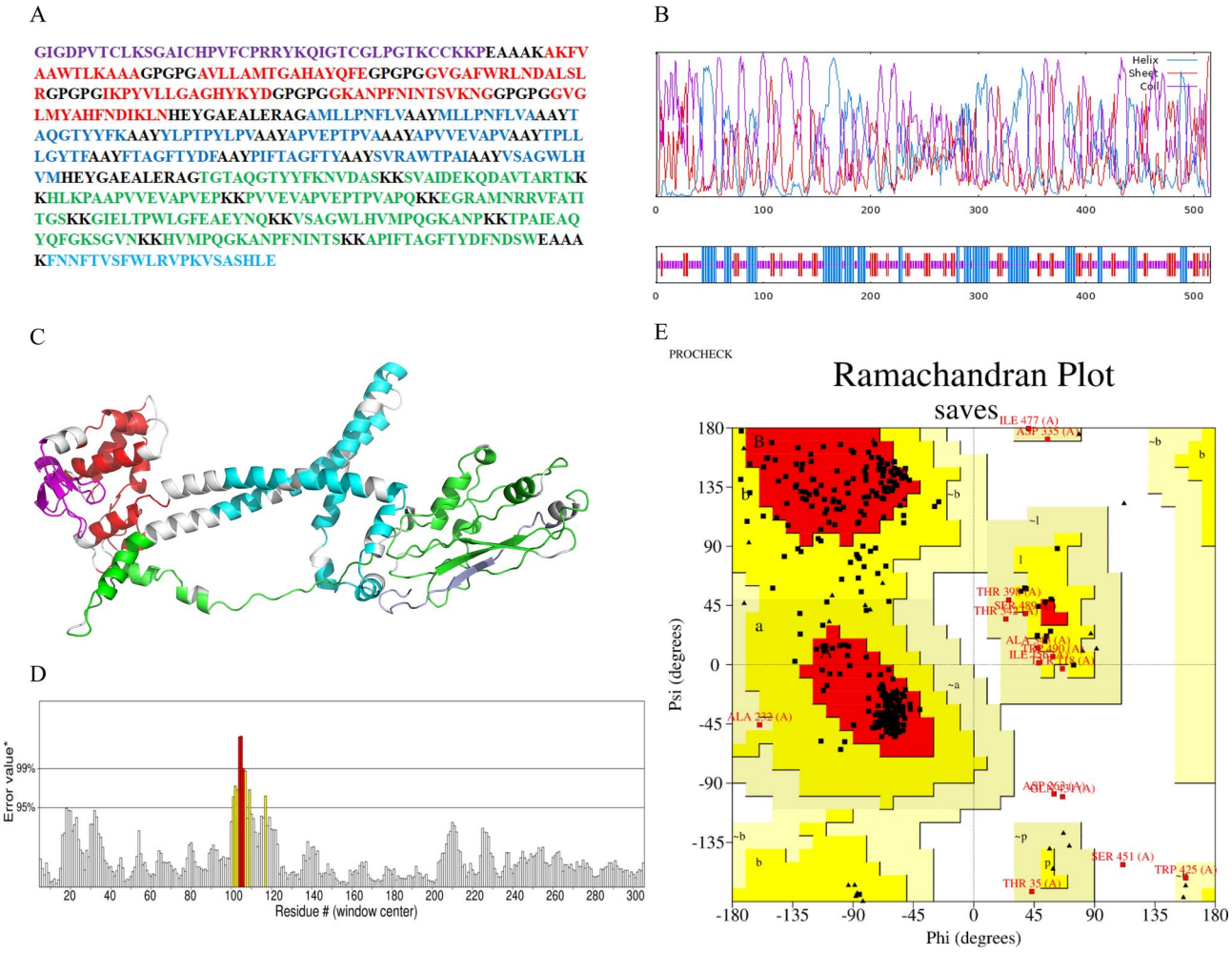

Fig. 2. Construction of multi-epitope vaccine. (**A**) Vaccine sequence of MEV, purple: β-defensin sequence, red: CTL epitopes, blue: HTL epitopes and PADRE sequence, green: linear B cell epitopes, lighter blue: p30 sequence, black: linkers. (**B**) secondary structure of MEV sequence, blue for helix, red for sheet, purple for coil. (**C**) tertiary structure of MEV, purple: β-defensin sequence, red: CTL epitopes, blue: HTL epitopes and PADRE sequence, green: linear B cell epitopes, lighter blue: p30 sequence, grey: linkers. (**D**) ERRAT score plot. (**E**) Ramchandran plots. (**F**) Prosa analyze of overall model quality.

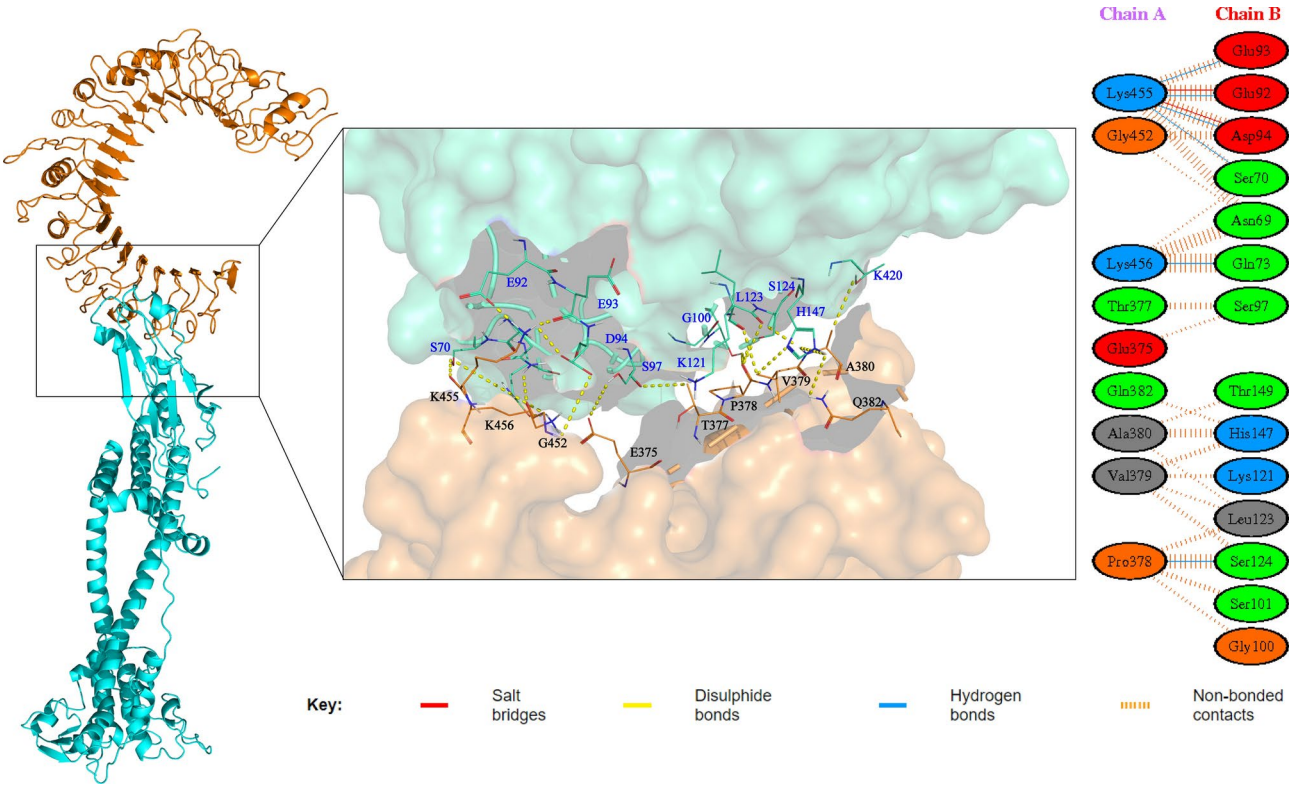

Fig. 3. Docking model of the vaccine with TLR2 molecule, blue represents the MEV molecule, and brown represents the TLR molecule.

sequence was integrated into the pET28a (+) plasmid between the BamHI and XhoI restriction sites for vector assembly (Figure S5).

Discussion

A. baumannii is a G-negative coccobacillus that thrives in aerobic environments. Over the last decade, substantial research progress has enhanced our comprehension of *A. baumannii*, elucidating its pathogenesis extensively[26]. The distinctive multidrug resistance exhibited by this pathogen has rendered our final line of defense against antibiotics, which includes carbapenems, colistin, and tigecycline, partially ineffective, and thus poses a significant global health threat[27]. Vaccine development is a vital strategy to counter such threat, vector and component vaccines offer superior targeting effects compared to live attenuated vaccines. The potential limitations of focusing on one single protein for vaccine development could result in providing only partial protection against infection.

Considering developing a vaccine centered on a single protein may offer only partial protection against infection[28], thus, we developed a multi-epitope subunit vaccine targeting the high prevalence of *Acinetobacter baumannii*. And through RNA engineering, the MEV sequence was designed to be a novel mRNA vaccine. An mRNA vaccine can offer enhanced protection by stimulating both T B cell responses in a balanced manner, thereby reducing the risk of integration into the host genome[29]. Moreover, mRNA vaccines have shown notable advantages in combating COVID-19, including versatile antigen design, straightforward preparation procedures, and the capacity for rapid production scaling[30].

Through reverse vaccinology screening of the *Acinetobacter baumannii* genome, three candidate target proteins were identified from the core genome, this reverse screening aids in the discovery of previously overlooked target proteins. Outer membrane proteins A (OmpA), W (OmpW), and 33–36 kDa Omp (Omp33-36) are porins located on the outer membrane of *A. baumannii*, playing a significant role in its pathogenicity. OmpW is a potential vaccine target with protective efficacy. In the sepsis model, both active and passive immunization against OmpW can effectively protect mice from *Acinetobacter baumannii* infection by significantly improving the survival rate, reducing the bacterial load in organs, and inhibiting the accumulation of inflammatory cytokines and chemokines in the serum[23]. OmpA also has potential protective efficacy. A DNA vaccine based on OmpA can protect mice from *Acinetobacter baumannii* infection, can prevent fatal bacterial challenges by reducing the bacterial load and pathological responses in the lungs[21]. They all play a significant role in the virulence and development of antibiotic resistance in *A. baumannii* by participating in crucial processes including adherence, invasion, apoptosis induction, serum resistance, biofilm formation, and persistence[6,24,31,32]. A total of 16 T cell epitopes (comprising 11 for CTL and 5 for HTL) along with 10 linear B cell epitopes were carefully chosen for the construction of the vaccine. These epitopes exhibit high conservation within multiple *A. baumannii* sequences, demonstrate robust antigenicity, and possess appropriate immunogenic properties. Also,

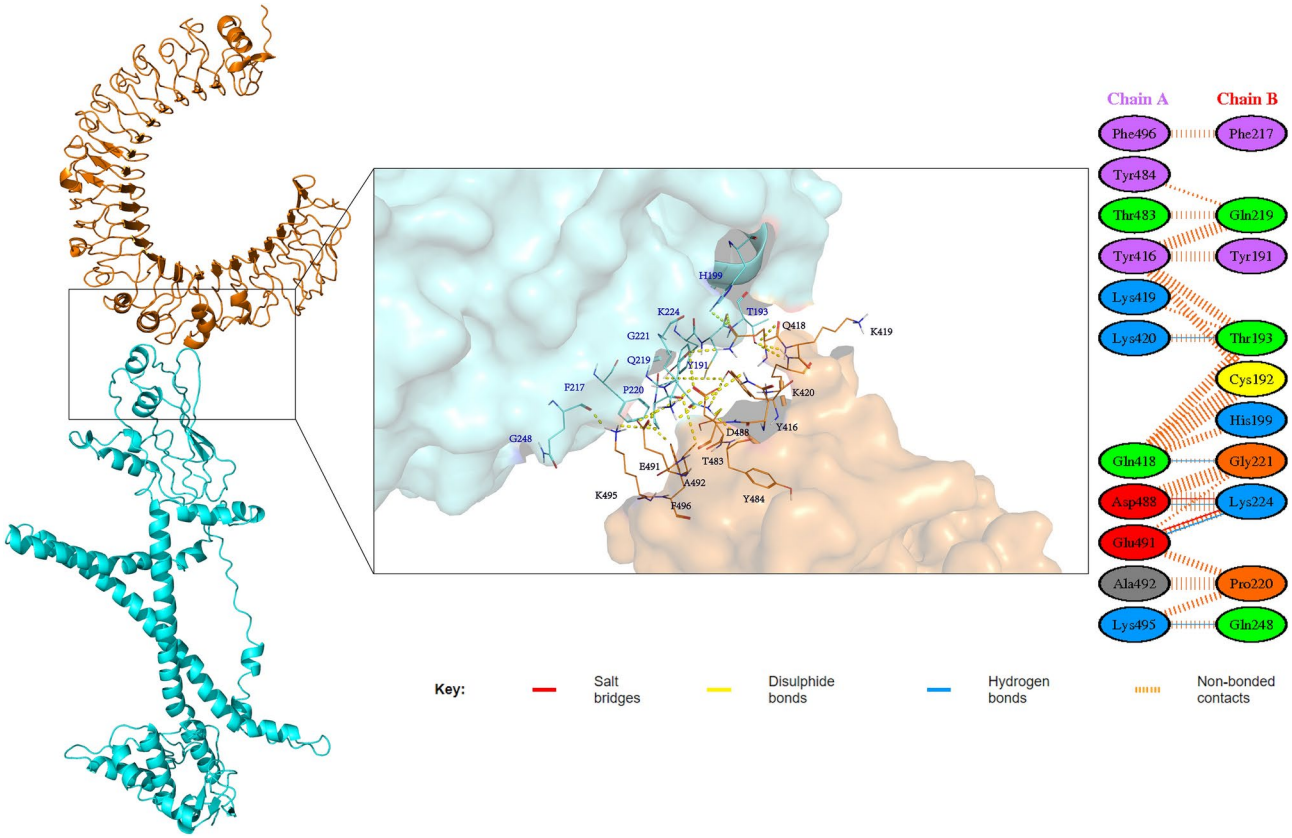

Fig. 4. Docking model of the vaccine with TLR4 molecule, blue represents the MEV molecule, and brown represents the TLR molecule.

there was no similarity observed between the selected epitopes and human or human gut commensal bacteria, mitigating the risk of triggering unintended autoimmune responses. To assemble the vaccine incorporating these epitopes, linkers including GPGPG, AAY, and KK connected the epitopes, GPGPG linker prevents the generation of junctional epitopes and facilitates the immune processing and presentation of the selected epitopes by HLA-II, thus used to connect HTL epitopes[33], while AAY linker help separate and align CTL epitopes effectively, as it has the function of a proteasome cleavage site that can be incorporated into proteins during the protein engineering process to enhance protein stability, folding, and expression levels[34]. And the KK linker can inhibit the production of antibodies directed against the peptide sequence generated by the linear connection of epitopes, thereby allowing the epitopes to maintain their distinct immunogenic activity[35]. Meanwhile, the specific HEYGAEALERAG linker functions as the interface between CTL and HTL epitopes, facilitating an effective connection and interaction between these two critical components of the vaccine[36]. Then, a PADRE epitope aimed at stimulating additional helper T cells was connected with other HTL epitopes. . With EAAAK linker, two adjuvants were connected to the epitope sequence, the EAAAK linker is a rigid connection help maintain flexibility and proper spacing between adjuvants and the vaccine, to ensure two components work together efficiently[37]. The attachment of β-defensin II regulates CTL and HTL responses as it plays a crucial role in the chemotaxis of Toll-like receptors (TLRs), particularly TLR2 and TLR4[38], while the P30 sequence from tetanus toxin serves as a highly effective CD4 + T epitope that enhances CD8 + CTL responses[39]. To substantiate the vaccine's ability to synthesize stable proteins and induce immune responses upon uptake by body cells, following the analyze of the physicochemical properties for the MEV's amino acid sequence, we utilized ab initio prediction method to determine the folding conformation of the protein in three-dimensional space. The Ramachandran plot and parameters such as Z-score were employed to assess the rationality of the protein's spatial structures. And the results indicated the stability of vaccine's structure.

Subsequently, the interactions between the MEV protein and immune receptors was validated through molecular docking. Given the crucial roles of TLR2 and TLR4 in pathogen recognition and the induction of inflammatory cytokines, we proceeded to conduct molecular docking experiments involving the vaccine protein and both TLR2 and TLR4. Our docking simulations consistently showed strong binding affinities between the vaccine molecules and the receptors. The ClusPro calculated the center weight score as -990 for the complex involving TLR2 and -1151 for the complex involving TLR4. In contrast, the HADDOCK algorithm yielded overall scores of -80.9 + /- 1.9 for the interaction with TLR2 and -83.5 + /- 0.7 for the interaction with TLR4. Analysis by PDBsum revealed the presence of 6 H-bonds and 2 salt bridges in MEV-TLR2 complex, while the MEV-TLR4 complex exhibited 5 H-bonds and 2 salt bridges. To further analyze docking results, we employed molecular dynamic simulation to model interactions within the MEV-receptor complexes in a water

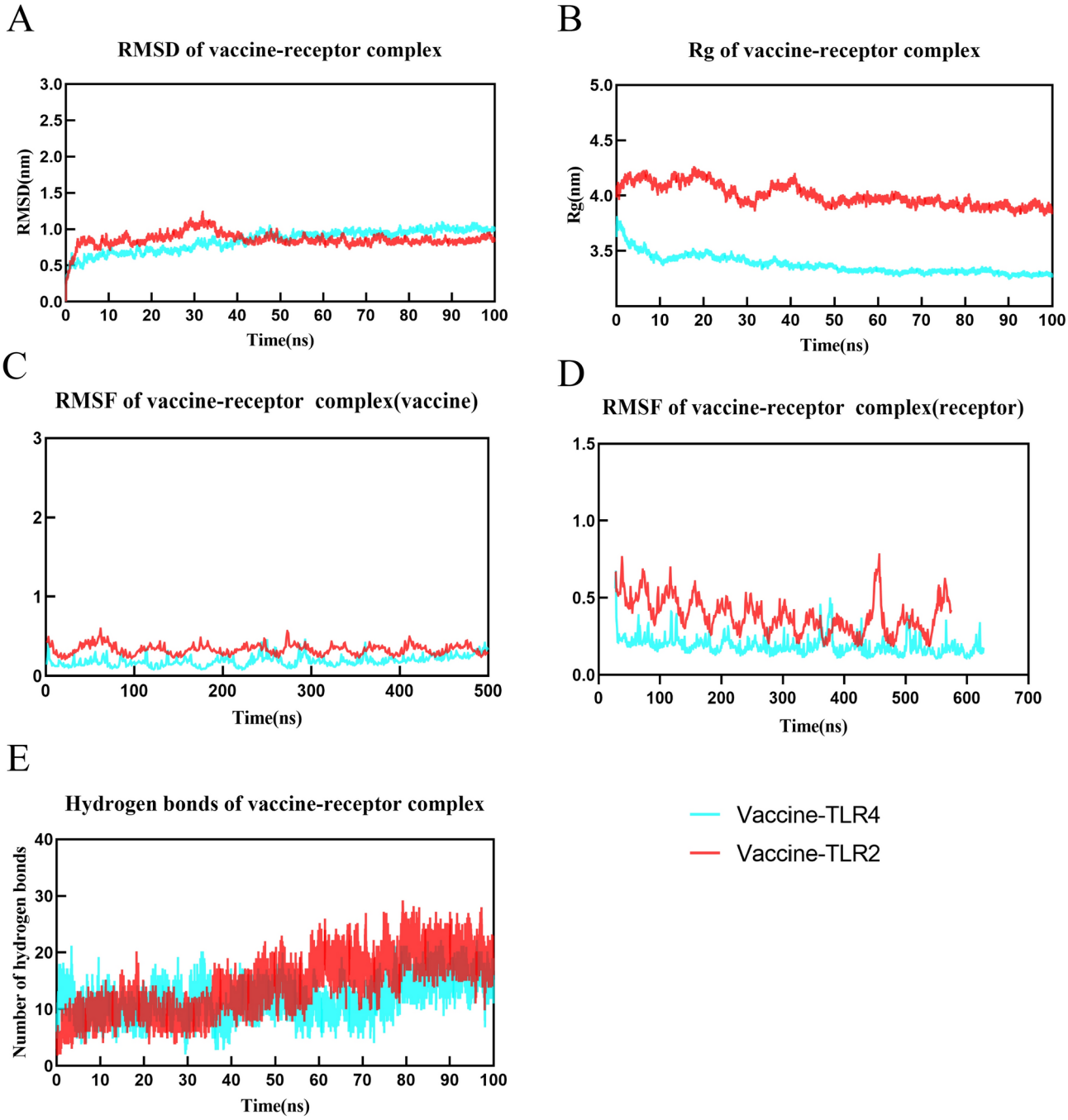

Fig. 5. Molecular dynamic simulation results. Blue for vaccine-TLR4 complex, red for vaccine-TLR2 complex. (**A**) RMSD (root mean square deviation) plots of vaccine-receptors, reflects the stability between the vaccine and receptor. (**B**) Radius of gyration (Rg) plots of vaccine-receptors complexes, suggesting the compactness of complexes. (**C**, **D**) RMSF (root mean square fluctuation) of vaccine-receptors, reflects the flexibility and fluctuation of the amino-acids residues in the side chain of docked complexes, vaccines' RMSF(C) and receptors' RMSF(D). (**E**) H-bonds formed in complexes.

environment. The 100 ns simulation revealed consistent interactions between the MEV and receptors, as shown by the RMSD analyses. Moreover, RMSF analysis unveiled residue flexibility, and Rg plots indicated complex dynamics, supporting the stability of the complexes. MM/GBSA estimation results aligned with the molecular dynamics findings, confirming strong binding affinities between the vaccine and the receptors.

Compared to the conventional approach to vaccine development, immunoinformatics-based vaccine design is more cost-effective and expedites epitope screening and vaccine formulation. Multiepitope vaccines offer reduced toxicity, fewer allergenic properties, and enhanced safety profiles compared to traditional vaccines. Our designed multiepitope vaccine includes CTL, HTL, and linear B cell epitopes, capable of eliciting both humoral

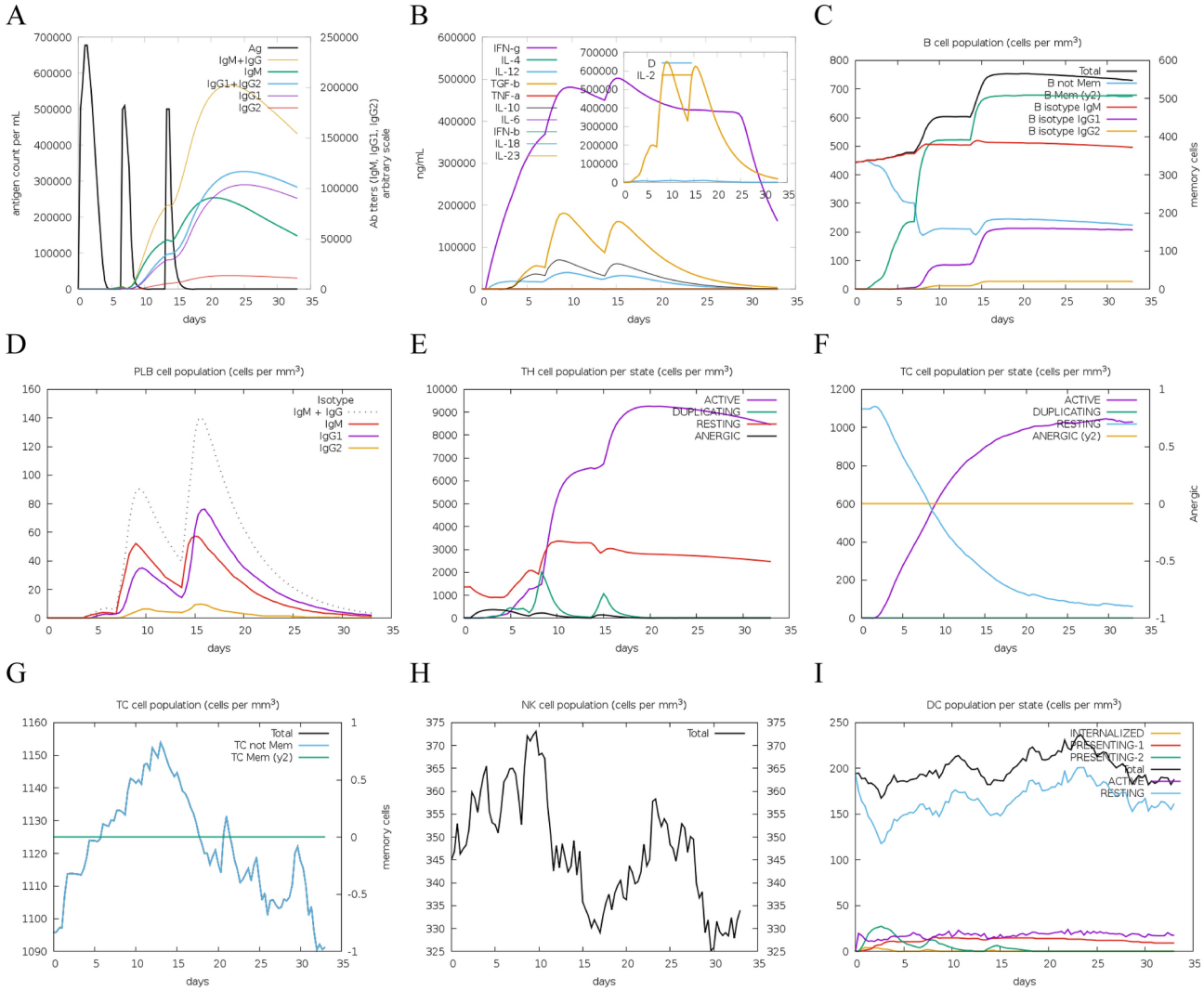

Fig. 6. Immunological simulation analysis. (**A**) Antibody levels induced by three doses of vaccine injection. (**B**) Levels of cytokines such as IL2, IFN-γ induced. (**C**) Levels of B cells induced. (**D**) Levels of plasma cells. (**E**) Levels of helper T (TH) cells induced. (**F**) Levels of cytotoxic T (TC) cells induced. (**G**) Levels of dendritic (DC) cells induced. (**H**) Levels of natural killer (NK) cells induced. (**I**) Levels of dendritic (DC) cells in different states.

and cellular immune responses. Moreover, the combined epitopes from distinct proteins demonstrate enhanced efficacy against *Acinetobacter baumannii* infections. Nevertheless, further in vivo and vitro validation for the MEV's performance against *Acinetobacter baumannii* is warranted.

Methods

Identification of target proteins through reverse vaccinology

The genome of *Acinetobacter baumannii* was analyzed using BPGA, from which core proteins were extracted[40]. Those core proteins were further selected with parameters below, the amino acid length should be more than 230 to cover multidomain and potentially multifunctional antigens[41]. Proteins with antigenicity > 0.5 were selected using VaxiJen, at this threshold, we can screen for proteins with antigenic potential[42,43], and proteins with multiple transmembrane domains predicted by TMHMM were excluded[44]. Proteins with high conservation and no homology to human proteins were selected through BLAST, combined with the studies of other researchers, ultimately determining three target proteins, OmpW, OmpA, Omp33-36[45]. Target protein sequences were obtained from NCBI database.

Use Molecular Evolutionary Genetics Analysis (MEGA) to conduct sequence alignment and draw phylogenetic trees for analyzing the evolutionary conservation of target proteins. All sequences of the three target proteins were obtained from NCBI refseq database, considering the sequences in refseq have undergone strict review and verification with higher accuracy and can better represent the real sequences proteins. After collecting the FASTA files of OmpA(507 sequences), OmpW(379 sequences) and Omp33-36(47 sequences) in batches from the NCBI, use the ClustalW method in MEGA to conduct alignment analysis for the subsequent

drawing of phylogenetic trees. The phylogenetic trees were draw with the method of Neighbor-Joining, and the bootstrap value was set to 1000.

T cell epitopes identification

The NetCTL 1.2 server effectively predicts cytotoxic T lymphocyte (CTL) epitopes by evaluating the binding of peptides to MHC class I molecules, the C-terminal cleavage process by the proteasome, and the efficiency of transport via the transporter associated with antigen processing (TAP)[46]. And we utilized the MHC-II Binding Predictions tool of IEDB along with the IEDB recommendation algorithm (NetMHCIIpan 4.1 EL) to identify the HTL epitopes[47]. The Vaxijen 2.0 tool was utilized to predict epitope antigenicity. Subsequently, epitopes with antigenicity scores greater than 0.4 were subjected to additional screening[42]. Moreover, the AllerTOP v2.0 and the ToxinPred servers was utilized to predict the allergenicity and toxicity of epitopes[48,49].

Epitopes ranking in the percentile below 2% were regarded as having a high affinity for binding to MHC II molecules. The activation of cytokines by helper T-cell epitopes is vital in adaptive immunity. The IFNepitope, IL4Pred, and IL10Pred servers were employed to assess the capacity of helper T-cell epitopes to stimulate IFN-γ, IL-4, and IL-10, respectively[50,51].

Identification of linear B cell epitopes

Using the ABCpred server, linear B cell epitopes were predicted with a threshold of 0.51, achieving an accuracy rate of 65.93%[52]. Subsequently, the VaxiJen 2.0, the AllerTOP, and the ToxinPred servers were employed to predict the antigenicity, allergenicity, and toxicity of the identified linear B cell epitopes. Only those linear B cell epitopes that exhibited favorable antigenicity and were non-toxic and non-allergenic were selected for further analysis.

Conservative and homology analysis

Collected full sequences of OmpA, OmpW, and Omp33 from NCBI. Clustal Omega was used to align various sequences, and Jalview was used to visualize the results[53]. The conservation of epitopes is expected to exceed 90% for MEV development. A BLAST analysis was conducted to ascertain homology between epitopes and human proteins, thereby reducing the likelihood of immune reactions against self-antigens[54].

Vaccine construct and calculation of physicochemical properties

The MEV sequence is composed of HTL, CTL, Linear B cell epitopes, as well as two adjuvants. AAY linkers were used to connect the CTL epitopes, GPGPG linkers for the HTL epitopes, and KK linkers for the linear B cell epitopes. Two HEYGAEALERAG linkers were placed in the gaps between HTL and CTL epitopes, and CTL and linear B cell epitopes. Adjuvant sequence β-defensin and P30 were separately connected to the N and C terminals of MEV sequence, with a linker of EAAAK[55]. Additionally, a pan HLA DR-binding epitope (PADRE) was integrated to enhance the induced adaptive immunity. The physicochemical properties of the MEV were evaluated with the ProtParam tool, which computed attributes such as theoretical isoelectric point (PI), instability index, aliphatic index, half-life, and hydrophilicity values. The antigenicity was evaluated using the VaxiJen and the ANTIGENpro server, while the allergenicity and toxicity were assessed with the AllerTOP and the ToxinPred server. The SOLpro (http://scratch.proteomics.ics.u-ci.edu/) was utilized to determine the vaccine's solubility probability when overexpressed in *E. coli*.

Secondary structure, tertiary structure prediction and refinement

GOR4 predicted the MEV's secondary structure, while the tertiary structure model was built with Robetta server (http://robetta.bakerlab.org/). Then, Galaxy-WEB (http://sysbio.rnet.missouri.edu/3Drefine/) was subsequently used to refine the tertiary model. Three key indicators—GDT-HA, RMSD, and MolProbity—were employed to assess the quality of the tertiary model[56]. Further, the model's quality can be assessed using the Procheck, ERRAT, and Pro-sa Web servers. A model is deemed high quality with an ERRAT score more than 85. And Z-score analyzed the overall quality of the MEV's tertiary structure, where a positive value signifies structural inaccuracies[57,58].

Conformational B cell epitopes prediction

The antibody epitope prediction tool ElliPro (http://tools.iedb.org/ellipro/) was employed for forecasting potential conformational B epitopes within vaccine structures. ElliPro delineates discontinuous antibody epitopes by utilizing the antigenic protein's 3D structure to assigns each anticipated epitope a corresponding protrusion index (PI) value[59].

Disulfide engineering of the vaccine construct

The Disulfide by Design 2.13 server (http://cptweb.cpt.wayne.edu/DbD2/index.php) was used to analyze the probably residue pairs that capable of forming disulfide bonds, these residue pairs are required to have the χ3 angle within the range of -87° or + 97° ± 10°, the Cα—Cβ—Sγ angle within the range of 114.6° ± 10°, and an energy value lower than 2.2 kcal/mol[60,61].

Molecular docking

Toll-like receptor 2 (TLR2) and Toll-like receptor 4 (TLR4) are important in recognizing viral membrane proteins and initiating the host's innate immune responses. The structures of TLR2 (PDB ID: 2Z7X) and TLR4 (PDB ID: 4G8A) were retrieved from the RCSB PDB database. Molecular docking of these molecules was conducted with reputable ClusPro 2.0, known for its accurate predictions of protein binding. Subsequently,

HADDOCK optimized and refined the structures of the protein complexes in a rational manner[62]. Lastly, the PDBsum analyzed the interactions between MEV and the receptors[63,64].

Molecular dynamic simulation

Processes of molecular dynamics simulation were conducted to investigate the stability of MEV-receptor complexes in aqueous solutions, aiming to elucidate the binding interactions between vaccines and receptors. The Gromacs v2022.1 software was utilized to perform 100 ns molecular dynamics simulations on all vaccine-receptor complexes using the Amber14SB force field. The complexes were placed in a cubic box filled with water molecules (TIP3P) and then neutralized by introducing Na + or Cl- ions. Next, energy minimization was carried out to achieve the lowest energy state of the protein complexes. The entire system was then equilibrated at 310 K, resembling body temperature, through 200 ps NVT (canonical ensemble) simulations. This was followed by 1 ns of NPT (isothermal-isobaric ensemble) simulations at 1 atm pressure. Finally, a 100 ns molecular dynamics simulation in aqueous solution at 310 K and 1 atm pressure using Gromacs was performed on the protein complex. RMSD (root mean square deviation), RMSF (root mean square fluctuation), the number of hydrogen bonds, and Rg (gyration radius) were analyzed based on the molecular dynamics simulation trajectory obtained through Gromacs[65].

MMPBSA (Molecular Mechanics/Poisson Boltzmann Surface Area) energy analysis

GMX_MMPBSA 1.56 computed the alterations in binding energy within protein complexes across simulated trajectories. The MMPBSA method was applied to evaluate the binding energies between protein molecules during the final 20 ns of the simulation, assuming the protein complex is in a stable configuration. The specific formula utilized for the calculations is as follows:

$$\Delta G^0_{0bind,solv} = \Delta G^0_{0bind,solv} + \Delta G^0_{solv,complex} - (\Delta G^0_{solv,ligand} + \Delta G^0_{solv,receptor}) \quad (1)$$

$$\Delta G^0_{solv} = \Delta G^0_{electrostatic,c=80} - \Delta G^0_{electrostatic,c=1} + \Delta G^0_{hydrophobic} \quad (2)$$

$$\Delta G^0_{vaccum} = \Delta E^0_{molecular\ mechanics} - T \bullet \Delta S^0_{normal\ mode\ analysis} \quad (3)$$

Populationg coverage and immune simulation

The frequencies of HLA alleles exhibit variation across diverse regions and populations. The Population Coverage Tool of IEDB website assessed the worldwide coverage of vaccines by considering the specific HLA molecules associated with different epitopes[66].

The C-IMMSIM (https://kraken.iac.rm.cnr.it/C-IMMSIM/index.php?page=0) simulated the host's immune responses following three vaccine injections with one week interval between each (as time 1, time 20 and time 40). By default, the HLA-A01:01, HLA-B07:02, and HLA-DRB1*01:01 allele gene molecules are chosen. Overall, the simulation lasts for a total of 35 days[67].

Construction of multi-epitope mRNA vaccine and secondary structure prediction

The Jcat server (http://www.jcat.de/Start.jsp) was employed for reverse translation and optimization of the vaccine. In order to create the final multi-epitope mRNA vaccine, the DNA sequence was adjusted by incorporating a Kozak sequence at the 5' end to improve RNA stability and translation efficiency[68]. Following the Kozak sequence, a signal peptide for Tissue Plasminogen Activator (tPA) was included to facilitate extracellular protein secretion and improve antigen presentation[69]. Additionally, an MHC I-targeting domain (MITD) sequence was added to the 3' end of the vaccine DNA sequence to aid in presenting CTL epitopes, with a TAA codon marking the end of translation[70]. To further stabilize the mRNA, a partial sequence of the cytomegalovirus immediate-early gene's Untranslated Region (UTR) was added as the 5' untranslated region, while a partial sequence of the human growth hormone served as the 3' UTR[71,72]. The complete DNA sequence was transcribed into mRNA using the Transcription Tool. Subsequently, the RNAfold server (http://rna.tbi.univie.ac.at/cgi-bin/RNAWebSuite/RNAfold.cgi) and mFold server (http://www.bioinfo.rpi.edu/applications/mfold) predicted the mRNA's secondary structure.

Vector construction

The Jcat server is used for reverse translation and codon optimization of vaccine sequences. Escherichia coli K12 was chosen as the host to avoid optimization of the cDNA sequence of the vaccine for the XhoI and BamHI restriction enzyme sites. The cDNA sequence was inserted into the pet28a (+) vector using SnapGene software.

Data availability

The data that support the findings of this study are available from the corresponding author, Pinhua Pan, upon reasonable request.

Received: 27 August 2024; Accepted: 27 December 2024
Published online: 09 January 2025

References

1. De Oliveira, D. M. P. et al. Antimicrobial resistance in ESKAPE pathogens. *Clin. Microbiol. Rev.* https://doi.org/10.1128/CMR.00181-19 (2020).
2. Peleg, A. Y., Seifert, H. & Paterson, D. L. Acinetobacter baumannii: emergence of a successful pathogen. *Clin. Microbiol. Rev.* **21**(3), 538–582 (2008).

3. Munoz-Price, L. S. & Weinstein, R. A. Acinetobacter infection. *N. Engl. J. Med.* **358**(12), 1271–1281 (2008).
4. Nasr, P. Genetics, epidemiology, and clinical manifestations of multidrug-resistant Acinetobacter baumannii. *J. Hosp. Infect.* **104**(1), 4–11 (2020).
5. Ramirez, M. S., Bonomo, R. A. & Tolmasky, M. E. Carbapenemases: Transforming acinetobacter baumannii into a yet more dangerous menace. *Biomolecules.* **10**(5), 720 (2020).
6. Lee, C. R. et al. Biology of Acinetobacter baumannii: Pathogenesis, antibiotic resistance mechanisms, and prospective treatment options. *Front. Cell Infect. Microbiol.* **7**, 55 (2017).
7. Kyriakidis, I., Vasileiou, E., Pana, Z. D. & Tragiannidis, A. Acinetobacter baumannii antibiotic resistance mechanisms. *Pathogens* **10**(3), 373 (2021).
8. Lob, S. H., Hoban, D. J., Sahm, D. F. & Badal, R. E. Regional differences and trends in antimicrobial susceptibility of Acinetobacter baumannii. *Int. J. Antimicrob. Agents.* **47**(4), 317–323 (2016).
9. Lotsch, F. et al. Epidemiological situation, laboratory capacity and preparedness for carbapenem-resistant Acinetobacter baumannii in Europe, 2019. *Euro Surveill.* https://doi.org/10.2807/1560-7917.ES.2020.25.45.2001735 (2020).
10. Ma, C. & McClean, S. Mapping global prevalence of Acinetobacter baumannii and recent vaccine development to tackle it. *Vaccines (Basel).* **9**(6), 570 (2021).
11. Meng, X. et al. Ten-year changes in bloodstream infection with Acinetobacter Baumannii complex in intensive care units in Eastern China: A retrospective cohort study. *Front. Med. (Lausanne).* **8**, 715213 (2021).
12. Gellings, P. S., Wilkins, A. A. & Morici, L. A. Recent advances in the pursuit of an effective Acinetobacter baumannii vaccine. *Pathogens.* **9**(12), 1066 (2020).
13. He, Y., Rappuoli, R., De Groot, A. S. & Chen, R. T. Emerging vaccine informatics. *J. Biomed. Biotechnol.* **2010**, 218590 (2010).
14. Oli, A. N. et al. Immunoinformatics and vaccine development: An overview. *Immunotargets Ther.* **9**, 13–30 (2020).
15. Zhang, Y. et al. Development and evaluation of a multi-epitope subunit vaccine against group B Streptococcus infection. *Emerg. Microbes Infect.* **11**(1), 2371–2382 (2022).
16. Dasari, V. et al. Lymph node targeted multi-epitope subunit vaccine promotes effective immunity to EBV in HLA-expressing mice. *Nat. Commun.* **14**(1), 4371 (2023).
17. McConnell, M. J., Rumbo, C., Bou, G. & Pachon, J. Outer membrane vesicles as an acellular vaccine against Acinetobacter baumannii. *Vaccine.* **29**(34), 5705–5710 (2011).
18. Nie, D. et al. Outer membrane protein A (OmpA) as a potential therapeutic target for Acinetobacter baumannii infection. *J. Biomed. Sci.* **27**(1), 26 (2020).
19. Luo, G. et al. Active and passive immunization protects against lethal, extreme drug resistant-Acinetobacter baumannii infection. *PLoS One.* **7**(1), e29446 (2012).
20. Zhang, X. et al. Mucosal immunization with purified OmpA elicited protective immunity against infections caused by multidrug-resistant Acinetobacter baumannii. *Microb. Pathog.* **96**, 20–25 (2016).
21. Lei, L. et al. DNA vaccine encoding OmpA and Pal from Acinetobacter baumannii efficiently protects mice against pulmonary infection. *Mol. Biol. Rep.* **46**(5), 5397–5408 (2019).
22. Huang, W. et al. Immunization with a 22-kDa outer membrane protein elicits protective immunity to multidrug-resistant Acinetobacter baumannii. *Sci. Rep.* **6**, 20724 (2016).
23. Huang, W. et al. OmpW is a potential target for eliciting protective immunity against Acinetobacter baumannii infections. *Vaccine.* **33**(36), 4479–4485 (2015).
24. Smani, Y., Dominguez-Herrera, J. & Pachon, J. Association of the outer membrane protein Omp33 with fitness and virulence of Acinetobacter baumannii. *J. Infect. Dis.* **208**(10), 1561–1570 (2013).
25. Pardi, N., Hogan, M. J., Porter, F. W. & Weissman, D. mRNA vaccines - a new era in vaccinology. *Nat. Rev. Drug Discov.* **17**(4), 261–279 (2018).
26. Morris, F. C., Dexter, C., Kostoulias, X., Uddin, M. I. & Peleg, A. Y. The mechanisms of disease caused by Acinetobacter baumannii. *Front. Microbiol.* **10**, 1601 (2019).
27. Asif, M., Alvi, I. A. & Rehman, S. U. Insight into Acinetobacter baumannii: pathogenesis, global resistance, mechanisms of resistance, treatment options, and alternative modalities. *Infect. Drug Resist.* **11**, 1249–1260 (2018).
28. McConnell, M. J. & Martin-Galiano, A. J. Designing multi-antigen vaccines against Acinetobacter baumannii using systemic approaches. *Front. Immunol.* **12**, 666742 (2021).
29. Liu, M. A. A comparison of plasmid DNA and mRNA as vaccine technologies. *Vaccines (Basel).* **7**(2), 37 (2019).
30. Polack, F. P. et al. Safety and efficacy of the BNT162b2 mRNA Covid-19 vaccine. *N. Engl. J. Med.* **383**(27), 2603–2615 (2020).
31. Uppalapati, S. R., Sett, A. & Pathania, R. The outer membrane proteins OmpA, CarO, and OprD of Acinetobacter baumannii confer a two-pronged defense in facilitating its success as a potent human pathogen. *Front. Microbiol.* **11**, 589234 (2020).
32. Novovic, K. et al. Acinetobacter spp. porin Omp33–36: Classification and transcriptional response to carbapenems and host cells. *PLoS One.* **13**(8), e0201608 (2018).
33. Farhani, I. et al. Designing a multi-epitope vaccine against the SARS-CoV-2 variant based on an immunoinformatics approach. *Curr. Comput. Aided Drug Des.* **20**(3), 274–290 (2024).
34. Ahmad, S. et al. Computational design of a multi-epitope vaccine candidate against Langya henipavirus using surface proteins. *J. Biomol. Struct. Dyn.* https://doi.org/10.1080/07391102.2023.2258403 (2023).
35. Sajjad, R., Ahmad, S. & Azam, S. S. In silico screening of antigenic B-cell derived T-cell epitopes and designing of a multi-epitope peptide vaccine for Acinetobacter nosocomialis. *J. Mol. Graph Model.* **94**, 107477 (2020).
36. Anwar, T. et al. Computational design of experimentally validated multi-epitopes vaccine against hepatitis E virus: An immunological approach. *PLoS One.* **18**(12), e0294663 (2023).
37. Ullah, A. et al. An in silico multi-epitopes vaccine ensemble and characterization against nosocomial Proteus penneri. *Mol Biotechnol.* (2023).
38. Mei, H. F. et al. beta-defensin 2 as an adjuvant promotes anti-melanoma immune responses and inhibits the growth of implanted murine melanoma in vivo. *PLoS One.* **7**(2), e31328 (2012).
39. Valmori, D. et al. Induction of a cytotoxic T cell response by co-injection of a T helper peptide and a cytotoxic T lymphocyte peptide in incomplete Freund's adjuvant (IFA): further enhancement by pre-injection of IFA alone. *Eur. J. Immunol.* **24**(6), 1458–1462 (1994).
40. Chaudhari, N. M., Gupta, V. K. & Dutta, C. BPGA- an ultra-fast pan-genome analysis pipeline. *Sci. Rep.* **6**, 24373 (2016).
41. Irudal, S. et al. Identification by reverse vaccinology of three virulence factors in burkholderia cenocepacia that may represent ideal vaccine antigens. *Vaccines (Basel).* **11**(6), 1039 (2023).
42. Doytchinova, I. A. & Flower, D. R. VaxiJen: a server for prediction of protective antigens, tumour antigens and subunit vaccines. *BMC Bioinformatics.* **8**, 4 (2007).
43. Dar, H. A. et al. Designing a multi-epitope vaccine against Mycobacteroides abscessus by pangenome-reverse vaccinology. *Sci. Rep.* **11**(1), 11197 (2021).
44. Krogh, A., Larsson, B., von Heijne, G. & Sonnhammer, E. L. Predicting transmembrane protein topology with a hidden Markov model: application to complete genomes. *J. Mol. Biol.* **305**(3), 567–580 (2001).
45. Altschul, S. F., Gish, W., Miller, W., Myers, E. W. & Lipman, D. J. Basic local alignment search tool. *J. Mol. Biol.* **215**(3), 403–410 (1990).

46. Larsen, M. V. et al. Large-scale validation of methods for cytotoxic T-lymphocyte epitope prediction. *BMC Bioinformatics.* **8**, 424 (2007).
47. Reynisson, B. et al. Improved prediction of MHC II antigen presentation through integration and motif deconvolution of mass spectrometry MHC eluted ligand data. *J. Proteome Res.* **19**(6), 2304–2315 (2020).
48. Dimitrov, I., Bangov, I., Flower, D. R. & Doytchinova, I. AllerTOP vol 2–a server for in silico prediction of allergens. *J. Mol. Model.* **20**(6), 2278 (2014).
49. Gupta, S. et al. In silico approach for predicting toxicity of peptides and proteins. *PLoS One.* **8**(9), e73957 (2013).
50. Dhanda, S. K., Gupta, S., Vir, P. & Raghava, G. P. Prediction of IL4 inducing peptides. *Clin. Dev. Immunol.* **2013**, 263952 (2013).
51. Dhanda, S. K., Vir, P. & Raghava, G. P. Designing of interferon-gamma inducing MHC class-II binders. *Biol. Direct.* **8**, 30 (2013).
52. Saha, S. & Raghava, G. P. Prediction of continuous B-cell epitopes in an antigen using recurrent neural network. *Proteins.* **65**(1), 40–48 (2006).
53. Madeira, F. et al. Search and sequence analysis tools services from EMBL-EBI in 2022. *Nucleic Acids Res.* https://doi.org/10.1093/nar/gkac240 (2022).
54. Chen, C. et al. A fast peptide match service for UniProt knowledgebase. *Bioinformatics.* **29**(21), 2808–2809 (2013).
55. Danila Valmori, J. F. R., Men, Y., Maryanski, J. L., Romero, P. & Corradin, G. Induction of a cytotoxic T cell response by co-injection of a T helper peptide and a cytotoxic T lymphocyte peptide in incomplete Freund's adjuvant (IFA): Further enhancement by pre-injection of IFA alone. *Eur. J. Immunol.* https://doi.org/10.1002/eji.1830240633 (1994).
56. Baek, M. et al. Accurate prediction of protein structures and interactions using a three-track neural network. *Science.* **373**(6557), 871–876 (2021).
57. Narang, P. K. et al. Functional annotation and sequence-structure characterization of a hypothetical protein putatively involved in carotenoid biosynthesis in microalgae. *South African J. Bot.* **141**, 219–226 (2021).
58. Wiederstein, M. & Sippl, M. J. ProSA-web: interactive web service for the recognition of errors in three-dimensional structures of proteins. *Nucleic Acids Res.* **35**(Web Server issue), W407–W410 (2007).
59. Ponomarenko, J. et al. ElliPro: a new structure-based tool for the prediction of antibody epitopes. *BMC Bioinformatics.* **9**, 514 (2008).
60. Craig, D. B. & Dombkowski, A. A. Disulfide by Design 2.0: a web-based tool for disulfide engineering in proteins. *BMC Bioinformatics.* **14**, 346 (2013).
61. Ahmad, S. et al. In silico design of a novel multi-epitope vaccine against HCV infection through immunoinformatics approaches. *Int. J. Biol. Macromol.* **267**(Pt 2), 131517 (2024).
62. Desta, I. T., Porter, K. A., Xia, B., Kozakov, D. & Vajda, S. Performance and its limits in rigid body protein-protein docking. *Structure.* **28**(9), 1071–81 e3 (2020).
63. Honorato, R. V. et al. Structural biology in the clouds: The WeNMR-EOSC ecosystem. *Front. Mol. Biosci.* **8**, 729513 (2021).
64. Laskowski, R. A., Jablonska, J., Pravda, L., Varekova, R. S. & Thornton, J. M. PDBsum: Structural summaries of PDB entries. *Protein Sci.* **27**(1), 129–134 (2018).
65. Kutzner, C. et al. GROMACS in the cloud: A global supercomputer to speed up alchemical drug design. *J. Chem. Inf. Model.* **62**(7), 1691–1711 (2022).
66. Bui, H. H. et al. Predicting population coverage of T-cell epitope-based diagnostics and vaccines. *BMC Bioinformatics.* **7**, 153 (2006).
67. Rapin, N., Lund, O., Bernaschi, M. & Castiglione, F. Computational immunology meets bioinformatics: the use of prediction tools for molecular binding in the simulation of the immune system. *PLoS One.* **5**(4), e9862 (2010).
68. Kim, S. C. et al. Modifications of mRNA vaccine structural elements for improving mRNA stability and translation efficiency. *Mol. Cell. Toxicol.* **18**(1), 1–8 (2022).
69. Kou, Y. et al. Tissue plasminogen activator (tPA) signal sequence enhances immunogenicity of MVA-based vaccine against tuberculosis. *Immunol. Lett.* **190**, 51–57 (2017).
70. Kreiter, S. et al. Increased antigen presentation efficiency by coupling antigens to MHC class I trafficking signals. *J. Immunol.* **180**(1), 309–318 (2008).
71. Rcheulishvili, N. et al. Designing multi-epitope mRNA construct as a universal influenza vaccine candidate for future epidemic/pandemic preparedness. *Int. J. Biol. Macromol.* **226**, 885–899 (2023).
72. Rybakova, Y. et al. mRNA delivery for therapeutic anti-HER2 antibody expression in vivo. *Mol. Ther.* **27**(8), 1415–1423 (2019).

Acknowledgements

Thanks to the support of W.Y.

Author contributions

Conceptualization, F.Z, and S.M.; methodology, F.Z.; validation, S.M. and Y.X., and Z.Z; formal analysis, P.Z, H.Y; writing—original draft preparation, S.M, Y.X and C.T; writing—review and editing: J.C; supervision, P.P and J.C.; project admin-istration, P.P and J.C; funding acquisition, P.P

Funding

This work is supported by 1. Key R&D Program of Hunan Province (No. 2022SK2038); 2. Natural Science Foundation of ChangSha(No.kq2208368); 3. Natural Science Foundation of Hunan Province of China (No.2023JJ30930); 4. The Scientific Research Program of FuRong Laboratory (No.2023SK2101); 5. National Natural Science Foundation of China (No. 81770080); 6. The National Natural Science Foundation of China (No. 8210012334); 7. Project Program of central south university graduate education teaching reform (No. 2022JGB025); 8. The national key clinical specialist construction programs of China (Grant Number z047-02); 9. Research Project of Teaching Reform in Colleges and Universities in Hunan Province (2021jy139-2); 10. China Postdoctoral Science Foundation (2022M713520); 11. Research Project on teaching reform of ordinary colleges and universities in Hunan province (2022JGYB037).

Declarations

Competing interests

The authors declare no competing interests.

Ethics approval and consent to participate
Not applicable.

Consent for publication
Not applicable.

Additional information
Supplementary Information The online version contains supplementary material available at https://doi.org/10.1038/s41598-024-84823-0.

Correspondence and requests for materials should be addressed to J.C. or P.P.

Reprints and permissions information is available at www.nature.com/reprints.

Publisher's note Springer Nature remains neutral with regard to jurisdictional claims in published maps and institutional affiliations.